

# Numerical computation of connecting orbits in delay differential equations

*Giovanni Samaey*  
*Koen Engelborghs*  
*Dirk Roose*

*Report TW 329, October 2001*



Katholieke Universiteit Leuven  
Department of Computer Science

Celestijnenlaan 200A – B-3001 Heverlee (Belgium)

# Numerical computation of connecting orbits in delay differential equations

*Giovanni Samaey*

*Koen Engelborghs*

*Dirk Roose*

*Report TW 329, October 2001*

Department of Computer Science, K.U.Leuven

## **Abstract**

We discuss the numerical computation of homoclinic and heteroclinic orbits in delay differential equations. Such connecting orbits are approximated using projection boundary conditions, which involve the stable and unstable manifolds of a steady state solution. The stable manifold of a steady state solution of a delay differential equation (DDE) is infinite-dimensional, a problem which we circumvent by reformulating the end conditions using a special bilinear form. The resulting boundary value problem is solved using a collocation method. We demonstrate results, showing homoclinic orbits in a model for neural activity and travelling wave solutions to the delayed Hodgkin-Huxley equation. Our numerical tests indicate convergence behaviour that corresponds to known theoretical results for ODEs and periodic boundary value problems for DDEs.

**Keywords :** delay differential equations, numerical bifurcation analysis, homoclinic and heteroclinic orbits

**AMS(MOS) Classification :** 65J15, 65P30

# Numerical computation of connecting orbits in delay differential equations

Giovanni Samaey, Koen Engelborghs and Dirk Roose

Department of Computer Science, Katholieke Universiteit Leuven,  
Celestijnenlaan 200A, B-3001 Heverlee-Leuven, Belgium

## Abstract

We discuss the numerical computation of homoclinic and heteroclinic orbits in delay differential equations. Such connecting orbits are approximated using projection boundary conditions, which involve the stable and unstable manifolds of a steady state solution. The stable manifold of a steady state solution of a delay differential equation (DDE) is infinite-dimensional, a problem which we circumvent by reformulating the end conditions using a special bilinear form. The resulting boundary value problem is solved using a collocation method. We demonstrate results, showing homoclinic orbits in a model for neural activity and travelling wave solutions to the delayed Hodgkin-Huxley equation. Our numerical tests indicate convergence behaviour that corresponds to known theoretical results for ODEs and periodic boundary value problems for DDEs.

**Keywords:** delay differential equations, numerical bifurcation analysis, homoclinic and heteroclinic orbits.

**AMS Subject Classifications:** 65J15, 65P30.

## 1 Introduction

In many applications, such as the investigation of global bifurcations or the computation of travelling wave solutions of (functional) partial differential equations, one is interested in computing homoclinic and heteroclinic orbits. This paper deals with the computation of such connecting orbits in systems of autonomous delay differential equations (DDEs),

$$\dot{x}(t) = f(x(t), x(t - \tau), \eta), \quad (1)$$

where  $\tau > 0$  is a (constant) delay,  $\eta \in \mathbb{R}^p$  represents a number of physical parameters, and  $f : \mathbb{R}^n \times \mathbb{R}^n \times \mathbb{R}^p \rightarrow \mathbb{R}^n$ . For notational convenience, we

only consider equations with a single delay, as generalization to the multiple delay case is straightforward.

We call a solution  $x^*(t)$  of (1) at  $\eta = \eta^*$  a *connecting orbit* if the limits

$$\lim_{t \rightarrow -\infty} x^*(t) = x^-, \quad \lim_{t \rightarrow +\infty} x^*(t) = x^+, \quad (2)$$

exist. For continuous  $f$ , these must be steady state solutions, i.e.

$$f(x^-, x^-, \eta^*) = f(x^+, x^+, \eta^*) = 0. \quad (3)$$

Homoclinic solutions, where  $x^- = x^+$ , typically arise in parameter-dependent problems as limiting cases of periodic orbits when the period tends to infinity [19, 24]. In two-parameter problems, it was shown for the ODE case that a branch of homoclinic solutions arises from a Takens-Bogdanov bifurcation [16]. The computation of both homoclinic and heteroclinic orbits is useful to study travelling wave solutions of (functional) partial differential equations [25, 26].

To compute connecting orbits in systems of ODEs, a boundary value problem formulation was proposed by Beyn [4]. Computation of these orbits is usually done with a collocation method, e.g. in AUTO [8] and its extension HomCont [5].

In this paper, we derive a boundary value problem (BVP) to compute connecting orbits in DDEs. We adapt the collocation methods that we developed for the computation of periodic solutions of DDEs [10, 12, 13]. The resulting routines are added to DDE-BIFTOOL [10, 14], a Matlab package for bifurcation analysis of DDEs. In Section 2 we introduce some basic notation and concepts about DDEs. In Section 3 we derive an appropriate boundary value problem. Its discretization, discussed in Section 4, yields a large system of non-linear equations, which we solve by a Newton method. Section 5 contains some implementation aspects. In Section 6, we address truncation and approximation errors and their effect on the accuracy of the solution. In Section 7 we use our method to compute homoclinic orbits in a model for neural activity. We illustrate the existence of Takens-Bogdanov points as origins of branches of homoclinic orbits. We also compute travelling wave solutions to the delayed Hodgkin-Huxley equation. In particular, we illustrate the dependence of the wave speed on the delay. Finally, Section 8 contains conclusions.

## 2 Preliminaries

Consider system (1) and let  $C_\tau := C([-\tau, 0]; \mathbb{R}^n)$  be the vector space of continuous functions mapping the interval  $[-\tau, 0]$  into  $\mathbb{R}^n$ . For  $s \in \mathbb{R}$ , denote by  $x_s^* \in C_\tau$  the segment of a solution  $x^*(t)$ , defined by

$$x_s^*(\theta) = x^*(s + \theta), \quad \theta \in [-\tau, 0].$$

$C_\tau$  is the state space for (1). That is, for any given  $s$ , the solution segment  $x_s^*$  uniquely determines  $x^*(t)$  for all  $t \geq s$ .

The linearization of (1) around a solution  $x^*(t)$  is the *variational equation* [17], given by

$$\dot{z}(t) = A_0(t)z(t) + A_1(t)z(t - \tau), \quad (4)$$

where, using  $f \equiv f(x^0, x^1, \eta)$ ,

$$A_i(t) := \frac{\partial f}{\partial x^i} \Big|_{(x^*(t), x^*(t-\tau), \eta)}, \quad i = 0, 1. \quad (5)$$

If  $x^*(t)$  corresponds to a steady state solution,  $x^*(t) \equiv x^* \in \mathbb{R}^n$ , with

$$f(x^*, x^*, \eta) = 0, \quad (6)$$

then the matrices  $A_i(t)$  are constant,  $A_i(t) \equiv A_i(x^*, \eta)$ . When we define the  $n \times n$ -di-mensional matrix  $\Delta$  as

$$\Delta(x^*, \eta, \lambda) := \lambda I - A_0 - A_1 e^{-\lambda\tau}, \quad (7)$$

we can write the *characteristic equation*,

$$\det(\Delta(x^*, \eta, \lambda)) = 0. \quad (8)$$

This equation has an infinite number of roots  $\lambda \in \mathbb{C}$  called the *characteristic roots*. We will also need the corresponding eigenvectors, so we write

$$\begin{cases} \Delta(x^*, \lambda, \eta)v = 0 \\ c^H v - 1 = 0 \end{cases} \quad (9)$$

or

$$\begin{cases} \Delta^H(x^*, \lambda, \eta)w = 0 \\ d^H w - 1 = 0, \end{cases} \quad (10)$$

where  $c$  and  $d$  are normalizing vectors.

We assume that all roots  $\lambda$  of (8) have multiplicity one, and that  $x^-$  and  $x^+$  are both hyperbolic, i.e. they have no characteristic root with zero real part. The associated right and left eigenfunctions are then given by  $\phi(\theta) = ve^{\lambda\theta}$ ,  $\theta \in [-\tau, 0]$ , resp.  $\psi(\theta) = w^H e^{-\lambda\theta}$ ,  $\theta \in [0, \tau]$ , with  $\phi(\theta) \in C([-\tau, 0]; \mathbb{C}^n)$  and  $\psi(\theta) \in C([0, \tau]; \mathbb{C}^{1 \times n})$  [17].

The steady state solution  $x^*$  is (asymptotically) stable if all characteristic roots have negative real part; otherwise it is unstable. Since the number of characteristic roots in any half plane  $\Re(\lambda) > \gamma$ ,  $\gamma \in \mathbb{R}$ , is finite [17], the stability is always determined by a finite number of roots.

### 3 Boundary value problem

In principle, a connecting orbit is defined by its profile  $x^*(t)$  on the real (time) axis. However, in order to compute it, this infinite domain has to be truncated to a finite length  $[0, T]$  and suitable boundary conditions must be applied. When we scale time by a factor  $T^{-1}$  and denote  $\bar{\tau} = \frac{\tau}{T}$ , this yields a boundary value problem,

$$\dot{y}(t) = Tf(y(t), y(t - \bar{\tau}), \eta), \quad \text{for } t \in [0, 1] \quad (11a)$$

$$b_-(y_1, x^-, \eta) = 0 \quad b_+(y_0, x^+, \eta) = 0 \quad (11b)$$

$$p(y, \eta) = 0 \quad (11c)$$

where  $b_- = 0$ , resp.  $b_+ = 0$ , represent the projection boundary conditions near the initial state  $x^-$  and final state  $x^+$ . Equation (11c) represents a suitable phase condition to remove translational invariance. A commonly used, robust phase condition [7] is given by

$$\int_0^1 u(t)u'_{k-1}(t)dt = 0. \quad (12)$$

This condition minimizes the phase shift of  $u(t)$  with respect to some (previous) solution  $u_{k-1}(t)$ . The latter is important when using adaptive meshes, to avoid the need for frequent remeshing.

We impose projection boundary conditions, as used in [4, 22] for ODEs. Formally, we require that the initial function segment  $y_0 \in C_{\bar{\tau}}$  lies in the linearization of the unstable manifold of  $x^-$  and that the final function segment  $y_1 \in C_{\bar{\tau}}$  lies in the linearization of the stable manifold of  $x^+$ . These conditions give rise to an overdetermined system, so it is necessary to free a number ( $n_\eta$ ) of the  $p$  physical parameters.

In order to derive conditions for the initial function segment, we repeat a theorem from [6].

**Theorem 1.** *Let  $y(t)$  be a solution of the linear DDE (1). For any  $\gamma \in \mathbb{R}$ , such that  $\det(\Delta(x^*, \lambda)) \neq 0$  on the line  $\Re(\lambda) = \gamma$ , we have the asymptotic expansion*

$$y(t) = \sum_{k=1}^l p_k(t)e^{\lambda_k t} + o(e^{\gamma t}) \text{ for } t \rightarrow +\infty, \quad (13)$$

where  $\lambda_1, \dots, \lambda_l$  are the (finitely many) zeros of  $\det(\Delta(x^*, \lambda)) = 0$  with real part exceeding  $\gamma$  and  $p_k(t)$  is a  $\mathbb{C}^n$ -valued polynomial in  $t$  of degree less than or equal to  $m_k - 1$ , with  $m_k$  the multiplicity of  $\lambda_k$  as a zero of  $\det(\Delta(x^*, \lambda))$ .

We use this theorem in the special case where  $\gamma = 0$  and all  $m_k = 1$ .

Suppose  $x^-$  has  $s^-$  distinct unstable eigenvalues  $\lambda_k^- > 0$ , with corresponding eigenvectors  $v_k^-$ , then the initial function segment can be written as

$$y_0\left(\frac{\theta}{T}\right) = x^- + \epsilon \sum_{k=1}^{s^-} \alpha_k v_k^- e^{\lambda_k^- \theta}, \quad (14)$$

with  $\sum_{i=1}^{s^-} |\alpha_k|^2 = 1$ . The steady state  $x^-$ , the eigenvalues  $\lambda_k^-$  and eigenvectors  $v_k^-$  are unknown, and have to be computed by adding equations (6) and (9). To ensure continuity at  $t = 0$ , the equation

$$y(0) = x^- + \epsilon \sum_{i=1}^{s^-} \alpha_k v_k^- \quad (15)$$

is added.

Unfortunately, we cannot use a similar expansion for the final function segment, because the stable manifold of a steady state of (1) is infinite-dimensional. However, for a steady state solution of (1), one can prove that the left eigenfunction  $\psi(\theta)$ , which belongs to the adjoint space  $C([0, \tau]; \mathbb{C}^{1 \times n})$ , is complementary to all right eigenfunctions  $\phi(\theta) \in C([-\tau, 0]; \mathbb{C}^n)$  under the special bilinear form

$$\langle \psi, \phi \rangle = \psi(0)\phi(0) + \int_{-\tau}^0 \psi(\xi + \tau) A_1(x^*, \eta) \phi(\xi) d\xi, \quad (16)$$

provided that  $\phi$  and  $\psi$  correspond to different eigenvalues [17]. In this equation,  $A_1(x^*, \eta)$  is defined by (5).

Hence, instead of writing the final function segment as an (infinite) sum of stable eigenfunctions, we require complementarity of the final function segment to all unstable eigenfunctions with respect to (16). That way, the final function segment is contained in the complement of the unstable manifold.

If  $x^+$  has  $s^+$  distinct unstable eigenvalues  $\lambda_k^+$  with corresponding left eigenvectors  $w_k^+$ , this leads to

$$w_k^{+H} (y(1) - x^+) + \int_{-\tau}^0 w_k^{+H} e^{-\lambda_k^+(\theta+\tau)} A_1(x^+, \eta) \left( y\left(1 + \frac{\theta}{T}\right) - x^+ \right) d\theta = 0 \quad (17)$$

for  $k = 1, \dots, s^+$ . Just as for the initial function segment, the unknown steady state  $x^+$ , the eigenvalues  $\lambda_k^+$  and eigenvectors  $w_k^+$  are determined by adding the equations (6) and (10).

## 4 Discretization

In order to compute an approximate solution to (11), we use a collocation method.

Let  $\Pi := \{0 = t_0 < t_1 < t_2 < \dots < t_L = 1\}$  be a mesh that partitions the interval  $[0, 1]$ , and let  $h_i = t_{i+1} - t_i$  for  $i = 0, \dots, L-1$ . Denote by  $\pi_m$  the set of all (vector-valued) polynomials of degree not exceeding  $m$ . We approximate a solution  $x^*(t)$  to (11) on the interval  $[0, 1]$  by an element  $u(t)$  from the following space of piecewise polynomials:

$$S_m(\Pi) := \{p \in C([0, 1], \mathbb{R}^n) : p|_{[t_i, t_{i+1}]} \in \pi_m, i = 0, \dots, L-1\}.$$

Clearly,  $\dim S_m(\Pi) = n \times (L \times m + 1)$ . Let  $X(\Pi) := \bigcup_{i=0}^{L-1} X_i$  with  $X_i := \{c_{i,l} := t_i + c_l h_i, l = 1, \dots, m\}$  be a given set of *collocation points* in  $[0, 1]$  based on the given, fixed set of *collocation parameters*  $\{c_l\}$  with  $0 \leq c_1 < c_2 < \dots < c_m \leq 1$ . Then the idea of a *collocation method* for approximating a solution to (11) is to find a function  $u(t) \in S_m(\Pi)$  that satisfies the system (11a) on the finite set  $X(\Pi)$ . The initial conditions (14) are used to evaluate the initial function segment,  $y(t), t \leq 0$ . The (integral) end conditions (17) are discretized with a Gauss quadrature rule of degree  $m$  on each subinterval  $[t_i, t_{i+1}]$  contained in  $[1 - \bar{\tau}, 1]$  and added as extra defining equations. Because  $1 - \bar{\tau}$  will generally not be a mesh point, we need to apply a suitable correction on the first such subinterval. We choose to use  $m$  Gauss points in the part of this subinterval that is used in the integration, i.e. on the part that is contained in  $[1 - \bar{\tau}, 1]$ .

For  $i = 0, \dots, L-1$ , the collocation solution can be represented on subinterval  $[t_i, t_{i+1}]$  as

$$p_i(t) = \sum_{j=0}^m u(t_{i+\frac{j}{m}}) \psi_{i,j}(t)$$

where

$$\psi_{i,j}(t) := \prod_{l=0, l \neq j}^m \frac{t - t_{i+\frac{l}{m}}}{t_{i+\frac{j}{m}} - t_{i+\frac{l}{m}}}, j = 1, \dots, m.$$

are Lagrange polynomials, and  $t_{i+\frac{j}{m}} = t_i + \frac{j}{m} h_i, j = 1, \dots, m-1$  are so-called *representation points*. Thus the collocation solution is completely characterized by  $u_{i+\frac{j}{m}} = p_i(t_{i+\frac{j}{m}}), i = 0, \dots, L-1, j = 0, \dots, m-1$  and  $u_L = p_{L-1}(1)$ .

This discretization yields the following large system of non-linear equations. Here  $\tilde{c}_{i,l} = c_{i,l} - \frac{\bar{\tau}}{h_i}, g_i$  denote the Gauss quadrature weighting factors,  $G$  denotes the total number of Gauss points used in the approximation of

(17), and  $k_{i,j}$  is chosen such that  $\tilde{c} \in [t_{k_{i,j}}, t_{k_{i,j}+1}]$ .

$$\sum_{j=0}^m u_{i+\frac{j}{m}} \dot{\psi}_{i,j}(c_{i,l}) = Tf\left(\sum_{j=0}^m u_{i+\frac{j}{m}} \psi_{i,j}(c_{i,l}), \sum_{j=0}^m u_{k_{i,j}+\frac{j}{m}} \psi_{k_{i,j},j}(\tilde{c}_{i,l}), \eta\right), \quad \tilde{c}_{i,l} > 0 \quad (18)$$

$$\sum_{j=0}^m u_{i+\frac{j}{m}} \dot{\psi}_{i,j}(c_{i,l}) = Tf\left(\sum_{j=0}^m u_{i+\frac{j}{m}} \psi_{i,j}(c_{i,l}), x^- + \epsilon \sum_{k=1}^{s^-} \alpha_k v_k^- e^{\lambda_k^- T \tilde{c}_{i,l}}, \eta\right), \quad \tilde{c}_{i,l} < 0 \quad (19)$$

$$(i = 0, \dots, L-1 \text{ and } l = 1, \dots, m)$$

$$f(x^-, x^-, \eta) = 0 \quad (20)$$

$$f(x^+, x^+, \eta) = 0 \quad (21)$$

$$\begin{aligned} \Delta(x^-, \lambda_v^-, \eta) v_k^- &= 0 \\ c_k^H v_k^- - 1 &= 0 \end{aligned} \quad (k = 1, \dots, s^-) \quad (22)$$

$$\begin{aligned} \Delta^H(x^+, \lambda_k^+, \eta) w_k^+ &= 0 \\ d_k^H w_k^+ - 1 &= 0 \end{aligned} \quad (k = 1, \dots, s^+) \quad (23)$$

$$\begin{aligned} w_k^{2H}(u(1) - x^+) + \sum_{i=1}^G g_i w_k^{+H} e^{-\lambda_k^+(\theta_i + \tau)} A_1(x^+, \eta) \left(u(1 + \frac{\theta_i}{T}) - x^+\right) &= 0 \\ &(k = 1, \dots, s^+) \end{aligned} \quad (24)$$

$$u_0 = x^- + \epsilon \sum_{i=1}^{s^-} \alpha_k v_k^- \quad (25)$$

$$\sum_{i=1}^{s^-} |\alpha_k|^2 = 1 \quad (26)$$

$$p(u, \eta) = 0 \quad (27)$$

This system is solved by a Newton-Raphson method, after linearization with respect to the unknowns listed in Table 1. The number of equations is  $nmL + 3n + (s^- + s^+)(n+1) + s^+ + 2$ . To obtain a generically isolated connecting orbit, we thus free  $n_\eta = s^+ - s^- + 1$  parameters.

We compute branches of connecting orbits with a classical continuation algorithm, namely by freeing one more parameter and using a pseudo-arclength parametrization [20].

| unknown             | dimension  |
|---------------------|--|
| $u_{i+\frac{j}{m}}$ | $(mL + 1)n$  |
| $T$                 | 1  |
| $\eta_i$            | $n_\eta$   |
| $x^-$               | $n$  |
| $x^+$               | $n$  |
| $\lambda_k^-$       | $s^-$  |
| $v_k^\perp$         | $s^+n$   |
| $\lambda_w^+$       | $s^+$  |
| $w_k^+$             | $s^+n$   |
| $\alpha_k$          | $s^-$  |
| total               | $nmL + 3n + (s^- + s^+)(n + 1) + s^- + n_\eta + 1$ |

Table 1: All unknowns of the large non-linear system (18)-(27), with their dimensions.

## 5 Implementation

### 5.1 Matrix structure

Figure 1 visualizes a possible matrix structure for the system of linear equations to be solved during each Newton iteration. This matrix contains a (large)  $mLn \times (mL + 1)n$  block, corresponding to the collocation equations and the unknown profile. This block is bordered by a number of rows and columns corresponding to the other equations and unknowns. The large block consists of a diagonal band, which itself is a concatenation of  $mn \times (m + 1)n$  blocks. The off-diagonal band is a consequence of the delay term. Because we use non-equidistant meshes, the distance between the diagonal band and the off-diagonal band is not fixed.

### 5.2 Initial guess

In order to solve system (18)-(27) with a Newton iteration, an initial guess must be provided. In the case of homoclinic orbits, an initial guess can easily be obtained from a periodic orbit with sufficiently large period. It can then be assumed that the profile is approximately constant in the neighbourhood of the steady state solution. The point where (an approximation of) the derivative of the first component of the profile is minimal, is corrected to a steady state for the parameter values of the periodic orbit. This steady state is used as a starting value for the steady state  $x^- = x^+$ . Its stability information (readily obtained within DDE-BIFTOOL) provides starting values for  $v_k^-$ ,  $w_k^+$  and  $\lambda_k^- = \lambda_k^+$ . To obtain starting values for  $\alpha_k$ , we project the initial point of the profile onto the unstable manifold of  $x^-$  and solve for  $\alpha_k$ . Normalization of the  $\alpha_k$  coefficients provides a starting value for  $\epsilon$ .

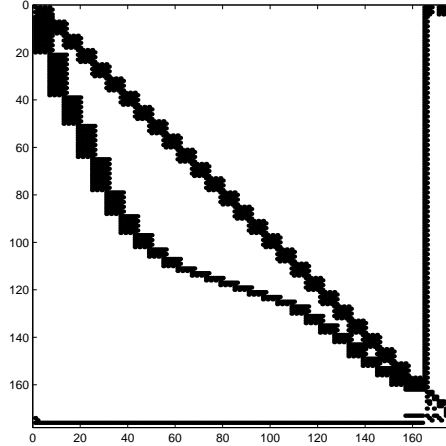


Figure 1: Typical structure of the Jacobian matrix arising in the Newton iteration. This example was obtained for model (40), see Section 7, using collocation polynomials of degree  $m = 3$  with  $n = 2$ ,  $L = 27$ ,  $\tau = 1$  and  $T \approx 10$ .

Obtaining a starting value for heteroclinic orbits is somewhat more difficult. One could use the method of successive continuation [9], adapted to the DDE case.

## 6 Convergence results

When computing connecting orbits using the procedure described above, two types of error occur. First, we truncate the infinite time domain to a finite interval of length  $T$ . Second, we compute an approximate solution using collocation. In this section, we investigate the effect of these approximations on the accuracy of the solution.

### 6.1 Truncation error

To examine the effect of truncation to a finite interval, we transform the interval  $[0, T]$  to an interval  $[T_-, T_+]$ , with  $T = T_+ + |T_-|$  and  $T_- \leq 0 < T_+$ . We define the profile error  $E_x(T)$ , the error on the parameters  $E_\eta(T)$  and the error on the unstable eigenvalues  $E_{\lambda^u}(T)$  as

$$E_x(T) = \max_{t \in [T_-, T_+]} \|y_T(Tt) - x^*(t)\| \quad (28)$$

$$E_\eta(T) = \|\eta_T - \eta^*\| \quad (29)$$

$$E_{\lambda^u}(T) = \|\lambda_T^u - \lambda^{u*}\|, \quad (30)$$

where  $(x^*(t), \eta^*)$  denotes the exact connecting orbit in (1) and  $(y_T(Tt), \eta_T)$  denotes the exact solution of the boundary value problem (11) when the

interval is truncated to a finite length  $T$ . We denote by  $\lambda^{u*}$  the real part of the unstable characteristic root of  $x^-$ , closest to the imaginary axis. That is,  $0 < \lambda^{u*} \leq \Re(\lambda)$  for all unstable eigenvalues  $\lambda$  of  $x^-$ . Similarly, let  $-\lambda^{s*}$  be the real part of the stable characteristic root of  $x^+$  closest to the imaginary axis, so  $\Re(\lambda) \leq -\lambda^{s*} < 0$  for all stable eigenvalues  $\lambda$  of  $x^+$ .

No theoretical results concerning the truncation error in the case of DDEs are known. Hence, we will compare the results of our numerical experiments with the truncation error bounds for the ODE case. In the latter case, the following bounds hold [4, 22].

**Theorem 2.** *Under suitable conditions on  $f$ , for  $|T_-|$  and  $T_+$  sufficiently large, and using projection boundary conditions, we have*

$$\begin{aligned} E_x(T) &= \mathcal{O}(\exp(-2 \min(\lambda^{u*}|T_-|, \lambda^{s*}T_+))) \\ E_\eta(T) &= \mathcal{O}(\exp(-\min((2\lambda^{u*} + \lambda^{s*})|T_-|, (2\lambda^{s*} + \lambda^{u*})T_+))) \\ E_{\lambda^u}(T) &= \mathcal{O}(\exp(-\min((2\lambda^{u*} + \lambda^{s*})|T_-|, (2\lambda^{s*} + \lambda^{u*})T_+))) \end{aligned}$$

When using other (e.g. periodic) boundary conditions, all exponents have to be divided by a factor 2.

As a test case, we consider the following system of two DDEs:

$$\begin{cases} \dot{x}_1(t) = x_2(t) \\ \dot{x}_2(t) = x_1(t) - x_1(t)x_1(t - \tau) + \eta x_2(t) + \mu x_1(t)x_2(t), \end{cases} \quad (31)$$

which has two steady states,  $(0, 0)$  and  $(1, 0)$ . This system (with  $\tau = 0$ ) was used in [4] to examine the effect of truncation for the computation of homoclinic orbits in ODEs. For convenience, we used the same model with an artificially introduced delay. We choose  $\mu = 0.5$  and  $\tau = 0.8255$ . In this case, a homoclinic orbit with saddle  $(0, 0)$  exists for  $\eta^* \approx -1.0796$ , see Figure 2.

The steady state  $(0, 0)$  has one unstable eigenvalue. The rightmost eigenvalues of this steady state are

$$\lambda^{u*} \approx 0.59695, \quad -\lambda^{s*} \approx -1.6752. \quad (32)$$

We perform a continuation in  $T$ , with  $\eta$  being a free parameter. To ensure that the truncation interval extends both towards  $-\infty$  and  $+\infty$  with increasing  $T$ , and to be able to compare results for different  $T$ , we choose  $T_+ = -T_- = \frac{T}{2}$  and we take  $x_2(0) = 0$  as a phase condition. For each  $T$  we solved the collocation equations with high accuracy ( $L = 250$  subintervals). Approximations of  $E_x(T)$ ,  $E_\eta(T)$  and  $E_{\lambda^{u*}}(T)$  are obtained by comparing solutions to a reference solution with  $T = 591.44$ . The results are shown in Table 2 and Figure 3. The following relations are clear:

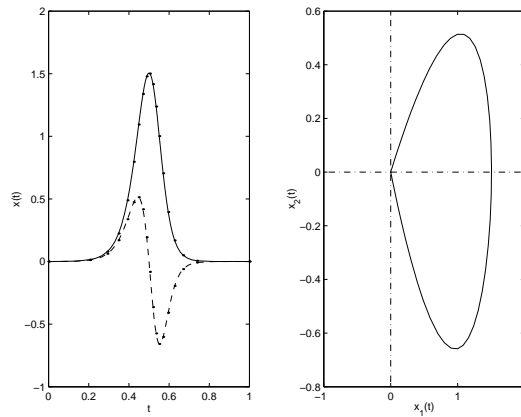


Figure 2: Left: Time profile of the homoclinic orbit of (31), where  $x_1(t)$  is solid and  $x_2(t)$  is dashed. Right: Phase portrait of the same homoclinic orbit.

|                        | observed<br>convergence order | expected<br>convergence order |
|------------------------|-------------------------------|-------------------------------|
| $E_x(T)$               | 0.609                         | 0.597                         |
| $E_\eta(T)$            | 1.389                         | 1.435                         |
| $E_{\lambda^{u^*}}(T)$ | 1.389                         | 1.435                         |

Table 2: Observed and expected convergence orders of system (18)-(27) with respect to increasing  $T$ .

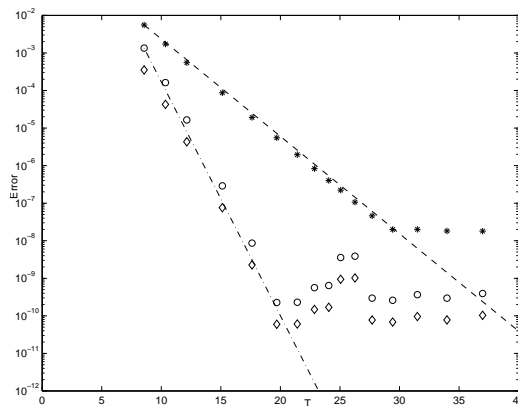


Figure 3: Truncation error for increasing  $T$  for the homoclinic orbit of (31).  $E_x(T)$  (\*),  $E_\eta(T)$ ( $\circ$ ) and  $E_{\lambda^{u^*}}(T)$ ( $\diamond$ ) are shown. As a reference, lines with slope  $-\lambda^{u^*}$  (-) and  $-\lambda^{u^*} + \frac{\lambda^{u^*}}{2}$  (-·-) are also shown, representing the theoretically known convergence behaviour for ODEs.

$$E_x(T) = \mathcal{O}(e^{-\lambda^{u^*}T}) \quad (33)$$

$$E_\eta(T) = \mathcal{O}(e^{(-\lambda^{u^*} + \frac{\lambda^{s^*}}{2})T}) \quad (34)$$

$$E_{\lambda^u}(T) = \mathcal{O}(e^{(-\lambda^{u^*} + \frac{\lambda^{s^*}}{2})T}) \quad (35)$$

Observe the superconvergent behaviour of  $E_\eta(T)$  and  $E_{\lambda^u}(T)$ . The apparent stagnation of convergence for  $T > 35$  is a consequence of the limited accuracy of the reference solution.

Since in our tests  $T = 2T_+ = 2|T_-|$ , these experimental results are in correspondence with Theorem 2. Hence, we conjecture that the known asymptotic convergence rates for homoclinic orbits with projection boundary conditions for ODEs remain valid in the case of DDEs.

## 6.2 Discretisation error

To show numerical convergence results for an increasing number of collocation points, we compute, for a given mesh, approximations of the continuous error  $E_c(h)$ , the discrete error  $E_d(h)$  and the error on the free parameters  $E_\eta(h)$ , defined by

$$E_c(h) := \max_{t \in [0,1]} \|y(t) - u_h(t)\| \quad (36)$$

$$E_d(h) := \max_{i=0, \dots, L} \|y(t_i) - u_h(t_i)\| \quad (37)$$

$$E_\eta(h) := \|\eta_y - \eta_{u_h}\|, \quad (38)$$

where  $y$  denotes the exact solution of the boundary value problem (11), and  $h$  denotes the width of the largest subinterval  $h = \max_i \{h_i\}$ .

As a test case, we consider the following system of two DDEs, modelling the interaction of two neurons [15]. Its bifurcation diagram is described in somewhat more detail in Section 7.

$$\begin{aligned} \dot{x}_1(t) &= -x_1(t) + q_{11} \frac{1}{1 + e^{-4x_1(t-\tau)}} - q_{12}x_2(t-\tau) + e_1 \\ \dot{x}_2(t) &= -x_2(t) + q_{21} \frac{1}{1 + e^{-4x_1(t-\tau)}} + e_2 \end{aligned} \quad (39)$$

This system has a homoclinic orbit for parameter values  $q_{11} = 2.6$ ,  $q_{12} = 1.45$ ,  $q_{21} = 1$ ,  $e_1 \approx -1.2963$ ,  $e_2 = -0.5$ ,  $\tau = 1$ . We approximate this trajectory with piecewise polynomials of degree  $m = 3$ , and we fix  $T \approx 120.1255$ . As a phase condition we fix  $x_2$  at  $t = \frac{T}{2}$ . The interval  $[0, T]$  is divided in  $L$  subintervals of equal width  $h = \frac{1}{L}$ , where  $L = 10, 11, \dots, 200$ . We choose Gauss-Legendre collocation points. As a reference solution, we compare with a solution obtained with  $L = 1000$  subintervals.

Figure 4 shows the evolution of the error with respect to the subinterval width  $h$ . We clearly observe an  $\mathcal{O}(h^{m+1})$  convergence behaviour, see also

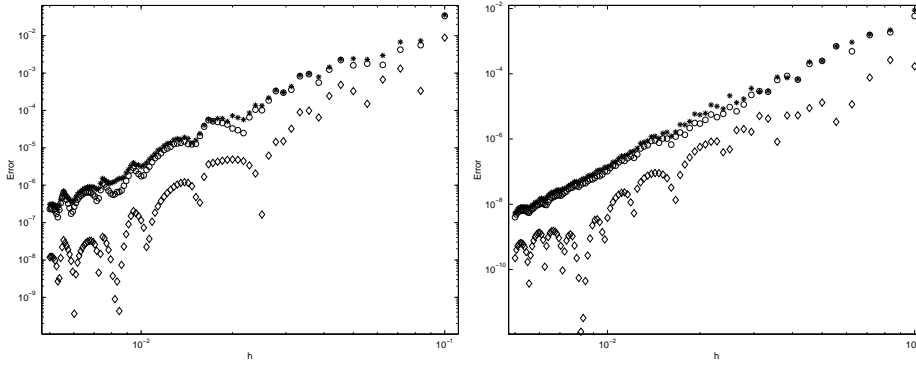


Figure 4: Evolution of  $E_c$  (\*),  $E_d$  (◦) and  $E_n$  (◇) in the case of system (39) with respect to the subinterval width  $h$ , when  $m = 3$  and  $m = 4$ , resp. , with Gauss-Legendre collocation parameters.

|       | $m = 3$ | $m = 4$ |
|-------|---------|---------|
| $E_c$ | 3.956   | 4.970   |
| $E_d$ | 4.030   | 4.932   |

Table 3: Numerical order of convergence in the case  $m = 3$  and  $m = 4$  with Gauss-Legendre collocation parameters, based on the errors for  $L = 30, \dots, 200$ .

Table 3. The convergence of the parameter is oscillatory, which prohibits an accurate estimate of the order of convergence. This result is in correspondence with similar results for collocation discretizations of initial value problems and periodic boundary value problems of DDEs [12, 2].

When computing difficult profiles, such as homoclinic orbits, one could expect better results when using adaptive meshes. For ODEs, an adaptive mesh selection strategy was proposed, based on a local error estimate [21, 1], which is implemented in AUTO [8] and proves to be very successful. Despite the fact that a local error estimate is not available for the DDE case, the same approach was also successful for the computation of periodic solutions of DDEs [13, 11] and is implemented in DDE-BIFTOOL.

We used the same adaptive mesh selection strategy for the computation of homoclinic orbits of DDEs. The results are shown in Figure 5. In this figure,  $\frac{1}{L}$  is used, in order to compare errors obtained using meshes of the same size. The error decrease indicates the effectivity of the approach for the current example. Similar results were observed on other examples.

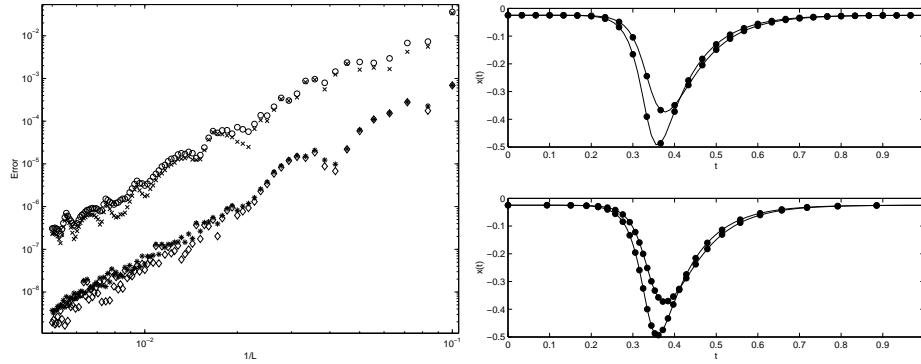


Figure 5: Left: Evolution for equidistant resp. adaptive meshes of  $E_c$  ( $\circ$  resp.  $*$ ),  $E_d$  ( $\times$  resp.  $\diamond$ ), in the case of system (39) with respect to  $\frac{1}{L}$ , when  $m = 3$  with Gauss-Legendre collocation parameters. The adaptive mesh is more accurate. Right above: Approximate solution with equidistant mesh. Right below: Approximate solution with adaptive mesh. The mesh adaptation procedure places more mesh points where the profile is steeper.

## 7 Examples

### 7.1 A model for neural activity

In [15], a model for the neural dynamics of a simple network consisting of two nerve cells, is given. It is described by the following system of two DDEs,

$$\begin{aligned} \dot{x}_1(t) &= -x_1(t) + q_{11} \frac{1}{1 + e^{-4x_1(t-\tau)}} - q_{12}x_2(t-\tau) + e_1 \\ \dot{x}_2(t) &= -x_2(t) + q_{21} \frac{1}{1 + e^{-4x_1(t-\tau)}} + e_2 \end{aligned} \quad (40)$$

Numerical computations have been performed using the parameter values,  $q_{11} = 2.6$ ,  $q_{21} = 1$  and  $e_2 = -0.5$  fixed. Parameters  $e_1$  and  $q_{12}$  are freed. Figure 6 shows a (partial) bifurcation diagram. We notice a number of codimension 2 bifurcations, which indicate that some of the known theoretical properties of ODEs generalize straightforwardly to the DDE case. Each of the two branches of Hopf points meets a branch of homoclinic orbits and the branch of fold points in a steady state solution with a double zero eigenvalue, indicating a Takens-Bogdanov point.

There is a double homoclinic orbit at the intersection of the two curves of homoclinic orbits, and two other branches of homoclinic orbits emanate from that point. This is shown in Figure 7.

Each of these branches of homoclinic orbits ends tangentially at a corres-

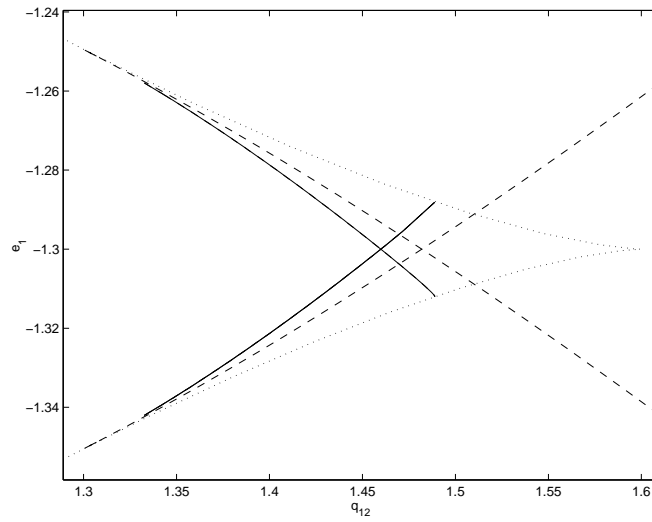


Figure 6: Partial bifurcation diagram for (40). The dotted line ('··') represents a fold curve, the dashed lines ('--') are branches Hopf points and the full lines are branches of homoclinic orbits.

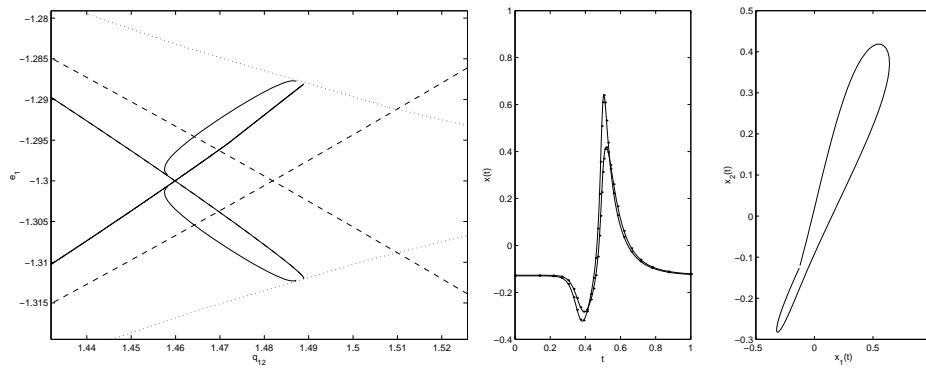


Figure 7: Left: A section of the bifurcation diagram of Figure 6, showing two additional branches of homoclinic orbits. Right: Trajectory of a homoclinic orbit for parameter values  $e_1 \approx -1.2881$  and  $q_{12} \approx 1.4838$  in the time domain and the phase plane, respectively.

ponding branch of fold points, in the same point as the other branch of homoclinic orbits. This indicates a saddle-node loop bifurcation point of codimension 2 [23].

## 7.2 Travelling waves in the delayed Hodgkin-Huxley equation

Consider the following reaction-diffusion equation [18]

$$\frac{\partial u(x, t)}{\partial t} = \frac{\partial^2 u(x, t)}{\partial x^2} + f(u(x, t), u(x, t - \tau), \eta), \quad (41)$$

where the reaction term  $f$  is of the delayed Hodgkin-Huxley type, i.e.  $f \equiv f(u^0, u^1, \eta)$  is defined as

$$f(u^0, u^1, \eta) := \begin{cases} u^0(1 - u^0)(u^1 - \eta) & \text{if } 0 \leq u^0 \leq 1, u^1 \in \mathbb{R} \\ u^0(1 - u^0)(u^0 - \eta) & \text{otherwise} \end{cases}$$

A travelling wave solution to this equation is a solution  $u(x, t)$  which travels at a constant speed  $c > 0$  without changing its shape. Therefore, it can be represented as  $u(x, t) = \zeta(x + ct)$ . It is stationary in the  $(s, t)$  coordinate system, where  $s = x + ct$ .

Theoretical work [26] shows the existence of travelling wave fronts for the Hodgkin-Huxley equation, with fixed limits  $\lim_{s \rightarrow -\infty} \zeta(s) = 0$  and  $\lim_{s \rightarrow +\infty} \zeta(s) = 1$ . In particular, it was proved that travelling waves exist for one specific speed  $c = c^* > 0$ , and that  $c^*$  is a monotonically decreasing function of the delay  $\tau$ .

The wave front profile  $\zeta(s)$  can be found by computing a connecting orbit from

$$\ddot{\zeta}(s) - c\dot{\zeta}(s) + f(\zeta(s), \zeta(s - c\tau), \eta) = 0,$$

and considering  $c$  as a physical parameter. We obtained an initial value for the solution of the non-linear system (18)-(27) at  $\tau = 0$  using time integration with the analytically known value for the parameter  $c$ .

For  $\eta = 0.25$ , the computed travelling wave profile for  $\tau = 0$  was continued in the direction of increasing delay. The results, shown in Figure 8, confirm the monotonical decrease of  $c^*$  with increasing delay.

## 8 Conclusions

Homoclinic orbits can be approximated by periodic orbits with large period. However, for the ODE case, it has been shown that the use of projection boundary conditions [4, 3, 22] offers several advantages: improved accuracy, the ability to compute heteroclinic orbits, and the availability of stability

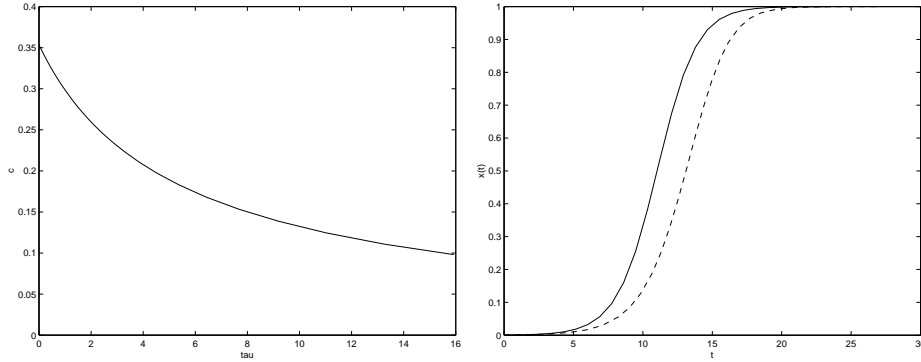


Figure 8: Left: the evolution of  $c^*$  in function of  $\tau$  for the equation (41) in the case  $\eta = 0.25$ . Right: wave profiles for  $\tau = 1$  (solid) and  $\tau = 16$  (dashed) for (41).

information of the connected stationary points (allowing detailed bifurcation analysis of the connecting orbits).

In this paper, we developed a method to compute connecting orbits in (systems of) DDEs based on projection boundary conditions. We circumvented the infinite-dimensional end condition (due to the infinite-dimensionality of the stable manifold of steady state solutions) by imposing these end conditions using a special bilinear form. The resulting method was incorporated in DDE-BIFTOOL, a Matlab package for bifurcation analysis of DDEs [14].

Numerical experiments indicate that the numerical properties of the method are comparable to those in the ODE case and that the adaptive mesh selection strategy used in DDE-BIFTOOL can be successfully applied.

We demonstrated the method using a DDE model for neural activity, showing the presence of a number of codimension 2 bifurcations along a branch of homoclinic orbits. We also computed travelling wave solutions of the delayed Hodgkin-Huxley equation, thereby confirming the (theoretically derived) dependence of wave speed on the delay.

## Acknowledgements

This research presents results of the Research Project OT 98/16, funded by the Research Council K.U.Leuven, of the Research Project G.0270.00 funded by the Fund for Scientific Research - Flanders (Belgium) and of the Research Project IUAP P4/02 funded by the programme on Interuniversity Poles of Attraction, initiated by the Belgian State, Prime Minister's Office for Science, Technology and Culture. The scientific responsibility is assumed by its authors. K. Engelborghs is a Postdoctoral Fellow of the Fund for Scientific Research - Flanders (Belgium).

## References

- [1] U. M. Ascher, R. M. M. Mattheij, and R. .D. Russell. *Numerical solution of boundary value problems for ordinary differential equations*. Prentice Hall, 1988.
- [2] A. Bellen. One-step collocation for delay differential equations. *J. Comput. Appl. Math.*, 10:275–283, 1984.
- [3] W. J. Beyn. The effect of discretization on homoclinic orbits. In T. Küpper, R. Seydel, and H. Troger, editors, *Bifurcation Analysis, Algorithms, Applications*, volume 79 of *ISNM*, pages 1–8. Birkhäuser, Stuttgart, 1987.
- [4] W. J. Beyn. The numerical computation of connecting orbits in dynamical systems. *IMA Journal of Numerical Analysis*, 9:379–405, 1990.
- [5] A. R. Champneys, Yu. A. Kuznetsov, and B. Sandstede. *A Numerical Toolbox for Homoclinic Bifurcation Analysis*. University of Bristol, 1995. Applied Nonlinear Mathematics Research Report No. 95.1.
- [6] O. Diekmann, S. A. Van Gils, S. M. Verduyn Lunel, and H.-O. Walther. *Delay equations: Functional-, Complex-, and Nonlinear Analysis*, volume 110 of *Applied Mathematical Sciences*, page 34. Springer-Verlag, 1995.
- [7] E. Doedel. Auto, a program for the automatic bifurcation analysis of autonomous systems. *Cong.Numer.*, pages 265–384, 1981.
- [8] E. J. Doedel, A. R. Champneys, T. F. Fairgrieve, Y. A. Kuznetsov, B. Sandstede, and X. Wang. *AUTO97: Continuation and Bifurcation Software for Ordinary Differential Equations (with HomCont)*, March 1998.
- [9] E. J. Doedel, M. J. Friedman, and B. I. Kunin. Successive continuation for locating connecting orbits. *Numerical Algorithms*, 17:103–124, 1997.
- [10] K. Engelborghs. DDE-BIFTOOL: a MatLab package for bifurcation analysis of delay differential equations. Technical Report TW-305, Dept. of Computer Science, KULeuven, March 2000.
- [11] K. Engelborghs. *Numerical Bifurcation Analysis of Delay Differential Equations*. PhD thesis, Katholieke Universiteit Leuven, May 2000.
- [12] K. Engelborghs and E. Doedel. Stability of piecewise polynomial collocation for computing periodic solutions of delay differential equations. *Numerische Mathematik*, 2001. Accepted.

- [13] K. Engelborghs, T. Luzyanina, K.J. in 't Hout, and D. Roose. Collocation methods for the computation of periodic solutions of delay differential equations. *SIAM J. Sci. Comput.*, 22(5):1593–1609, 2000.
- [14] K. Engelborghs, T. Luzyanina, and D. Roose. Numerical bifurcation analysis of delay differential equations using DDE-BIFTOOL. Submitted, 2001.
- [15] F. Giannakopoulos and O. Oster. Bifurcation properties of a planar system modelling neural activity. *J. Differential Equations Dynam. Systems*, 5(3/4), 1997.
- [16] J. Guckenheimer and P. Holmes. *Nonlinear Oscillations, Dynamical Systems and Bifurcations of Vectorfields*. Springer Verlag, 1993.
- [17] J. K. Hale. *Theory of Functional Differential Equations*, volume 3 of *Applied Mathematical Sciences*. Springer-Verlag, 1977.
- [18] A. L. Hodgkin and A. F. Huxley. A quantitative description of membrane current and its application to conduction and excitation in nerve. *J. Physiol.*, 117:500–544, 1952.
- [19] Yu. Kuznetsov. *Elements of applied bifurcation theory*, volume 115 of *Applied Mathematical Sciences*. Springer-Verlag, 1995.
- [20] L. Liu, G. Moore, and R. D. Russell. Computation and continuation of homoclinic and heteroclinic orbits with arclength parametrisation. *SIAM Journal of Scientific Computing*, 18(1):69–93, 1997.
- [21] R. D. Russell and J. Christiansen. Adaptive mesh selection strategies for solving boundary value problems. *SIAM J. Numer. Anal.*, 15(1), 1978.
- [22] B. Sandstede. Convergence estimates for the numerical approximation of homoclinic solutions. *IMA Journal of Numerical Analysis*, 17:437–462, 1997.
- [23] S. Schecter. The saddle-node separatrix-loop bifurcation. *SIAM J. Math. Anal.*, 18(4), July 1987.
- [24] R. Seydel. *Practical Bifurcation and Stability Analysis*, volume 5 of *Interdisciplinary Applied Mathematics*. Springer-Verlag, second edition, 1994.
- [25] A. Volpert, V. Volpert, and V. Volpert. *Travelling Wave Solutions of Parabolic Systems*, volume 140 of *Trans. Math. Monographs*. AMS, 1994. Providence.

- [26] J. Wu. *Theory and Applications of Partial Functional Differential Equations*, volume 119 of *Applied Mathematical Sciences*. Springer, 1996.